Article

Innovative One-Shot Paradigm to Tune Filler−Polymer Matrix Interface Properties by Plasma Polymer Coating in Osteosynthesis Applications

Xavier Carette, Laeticia Dhond, Axel Hemberg, Damien Thiry, Rosica Mincheva,* Jonathan Cailloux, Orlando Santana Perez, Damien Cossement, Marie Dubus, Halima Kerdjoudj, Rony Snyders, and Jean-Marie Raquez*
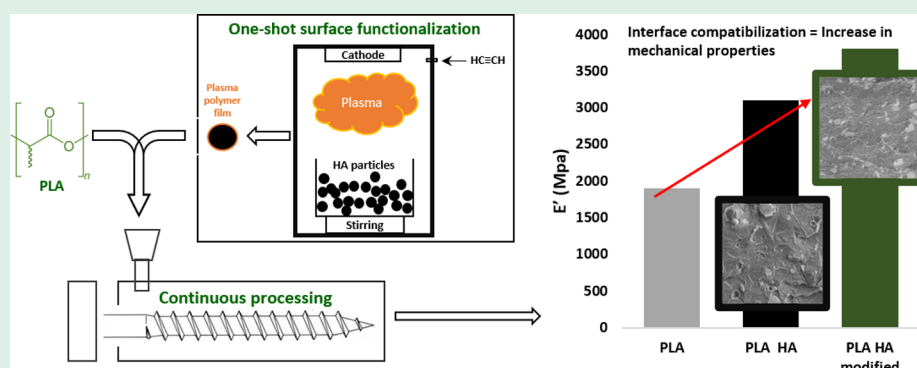
Read Online

ACCESS | Metrics & More | Article Recommendations | Supporting Information

ABSTRACT: The present study aims to improve the interfacial bonding between hydroxyapatite particles (HAs) and polylactide (PLA) to enhance the mechanical performance and biocompatibility of bone implants based on HA/PLA. For this, one-shot surface functionalization of HA via plasma polymerization is developed. Taking advantage of acetylene plasma chemistry, the hydrophobicity of HA particles was finely tuned prior to their introduction into a PLA matrix via an extrusion process. The effect of the plasma power (20 or 100 W) on the composition of the plasma polymer film (PPF) formed on the HA surface was studied via Fourier transform infrared (FTIR) spectroscopy, time-of-flight secondary-ion mass spectrometry (ToF-SIMS), and X-ray photoelectron spectroscopy (XPS). The amount of PPF formed was evaluated via thermogravimetric analyses (TGA). Cytotoxicity of the modified HA particles was monitored by the WST-1 proliferation assay and lactate dehydrogenase (LDH) release and showed that independent on the studied conditions, cell viability remained above the 70% threshold and LDH accumulation changes were insignificant, suggesting good biocompatibility. Contact angle measurements and morphological and rheological analyses showed that the low working power promoted more hydrophobic surfaces and a better HA/PLA interface. Dynamic mechanical analyses revealed that the storage modulus at 37 °C increased for the composite containing functionalized particles by 1.5 times compared to the neat particle's composites. This work opens a route toward further one-shot development of improved scaffolds for bone tissue engineering.

KEYWORDS: one-shot surface functionalization, plasma polymerization, interfacial compatibilization, PLA, HAP, viscoelastic properties, cytotoxicity

INTRODUCTION

Calcium phosphate-based materials (mainly hydroxyapatite, HA) have been widely used in bone-regenerative medicine due to their ability to induce bone formation. Despite the osteoconductive properties, the brittle, fragile, and inherent hardness of HA induces difficulty in the processing and proper shaping of implants, particularly in patients with extensive bone trauma, disease, and/or advanced age. Furthermore, HA friability and poor strength often limit its use in load-bearing applications. To overcome these limitations, HA micro- and nanoparticles were combined with different polymers to produce organic−inorganic composites for bone-reconstructive applications.[1,2] This combination allows ease of processing and

shaping as well as mechanical integrity preservation for the desired period.

Among the used polymers, poly(lactic acid) (PLA), a biocompatible and biodegradable polyester[3,4] with a controllable degradation rate in vivo through the hydrolysis of ester bonds,[5] was extensively studied in HA biocomposites. It was expected that their fabrication will synergistically reinforce the relatively low-modulus polymer with a high-modulus, high-strength inorganic material and that the plastic flow of the polymeric material under stress will transfer the load to the reinforcing phase.[6,7] Intuitively, such results are dependent on the filler–polymer interactions at the interface, e.g., on the control of the relative volume fraction of each phase that can be obtained by ensuring the dispersion and distribution of the ceramic filler within the polymer phase. The interfacial bond strength needs to be sufficient to transfer the load from the matrix to the filler. Any filler agglomeration is undesirable and may act as a stress initiator and stress concentrator and trigger the failure of a material. Practically, this is the case for PLA/HA composites, where agglomeration of HA particles in the PLA matrix is observed because of the poor interfacial affinity between the hydrophilic HA and hydrophobic PLA.[8] Multiple investigations have shown that only physical adsorption is achieved between HA and PLA.[9−12] Since the forces determining the mode of failure in reinforced composites are concentrated in a nanoscale mode,[13,14] maximum reinforcement will only be achieved if the particles are well bonded and well dispersed in the matrix through a nanoscale interface. Keeping this in mind, a number of innovative approaches were tested in the literature, mostly dealing with HA surface modification.[6]

The surface of the HA particles can be modified to improve this interfacial bonding by using surfactants such as oleic acid,[15] synthetic polyelectrolytes,[16] and heparin.[17] This methodology is found to induce hydrophobicity and improve the mechanical properties of the composite. However, the plasticizing effect[18] is often related to a decrease of the overall mechanical properties and negative effects for load-bearing applications. The grafting of polymer on the HA surface is an alternative with or without a linker through grafting to[19] or grafting from[20,21] techniques. In this context, the plasma polymerization process appears to be a suitable method for finely tuning surface properties.

Briefly, the formation of a layer of the plasma polymer film (PPF) includes the production of reactive species (i.e., ions and mainly radicals) in a gas phase and their subsequent condensation on the surface exposed to the plasma.[22−24] The generated complex growth mechanism involving a multitude of surface and gas-phase reactions is responsible for the uniqueness of PPF such as the absence of repeating units in contrast with conventional polymers and, most of the time, a highly cross-linked network formation at the modified surface. These specific features can lead to very attractive physicochemical properties: adhesion on almost all kinds of substrates even with complex shapes (i.e., micro/nanoparticles,[25] nanofibers,[26] etc.), high thermal stability, and insolubility in most of the solvents. Moreover, the process is also highly versatile, enabling the modulation of the surface properties in a wide range and can also be transferred at an industrial scale. It has been recently shown that acrylic acid and ε-caprolactone PPF deposited on the surface of HA particles[27] enable us to tailor the wettability and the mechanical properties of the material to some extent by adjusting the process parameters.[28] However, a two-step treatment was required to activate the surface with an oxygenated plasma before the introduction of the precursor.

In this work, on this basis, we report on a one-step method based on the plasma polymerization of acetylene to tune up the surface properties of micron-scale particles of HA. The influence of the power dissipated in the plasma on the physicochemical properties of the PPF is investigated by combining several characterization techniques (Fourier transform infrared (FTIR) spectroscopy, time-of-flight secondary-ion mass spectrometry (ToF-SIMS), water contact angle (WCA)). The cytotoxicity of the plasma-modified HA particles is also examined. The composites are prepared by the solvent-free extrusion process. The performance of the composites and the quality of the filler/matrix interface were analyzed by scanning electron microscopy (SEM), dynamical mechanical analysis (DMA), and rheology measurements.

■ MATERIALS AND METHODS

Materials. The poly(lactic acid) (PLA) used for this research is NatureWorks Ingeo Biopolymer 4060D (M_w = 120 000 g/mol), with a density of 1.24 g/cm³. PLA has no melting point temperature, but the working temperature is between 180 and 210 °C. Hydroxyapatite powder of 10 μm with a specific area of 100 m²/g was purchased from Aldrich and used as received. The synthesis-grade $CHCl_3$ was procured from VWR and used without purification. Acetylene gas was purchased from air-liquid with purity above 99.5%.

Methods. *HA Surface Modification via Plasma Polymerization.* Plasma polymerization is carried out in a cylindrical stainless vacuum chamber. The pumping of the reactor is made by a combination of a turbomolecular pump in series with a primary pump, allowing to reach a residual pressure of ~2 × 10⁻⁷ Torr (10⁻⁵ Pa). The plasma is produced through an ENI RPG asymmetric bipolar pulsed DC power supply (operating at a frequency of 250 kHz and a reverse pulse duration of 1616 ns) connected to a graphite target (99% purity, 2″ in diameter) in a C_2H_2 atmosphere. For all of the experiments, the precursor flow rate and the working pressure (controlled through a throttle valve connected to a capacitive gauge) were fixed to 40 sccm and 10 mTorr, respectively. In this work, two power (P) values applied to the cathode are studied: 20 and 100 W. For the characterization of the physicochemical properties of the PPF, the depositions were made on silicon wafer (001 orientation) substrates located in front of the graphite target. Regarding the deposition on HA microparticles, a powder (2.5 g) was placed in a cylindrical ceramic crucible on the sample holder. A loudspeaker was set below the holder to induce vibration and hence the mixing of the powder during the plasma deposition, thus ensuring a homogeneous coating of the particles (Figure S1). The treated powder was then removed from the chamber and sieved by an A200 Digit RETSH.

Composite Preparation. Prior to mixing, a masterbatch is realized in $CHCl_3$ with the particles and PLA. The masterbatch is dried overnight at 50 °C under a vacuum to remove the residual solvent. PLA pellets were dried overnight at 60 °C under vacuum. The composites were prepared by a vertical extrusion process at 180 °C with a microextruder of 15 cm³ (DSM, Xplore). The materials were introduced at 30 rpm for 2 min, followed by a mixing step of 4 min at 75 rpm. The final materials were shaped into specific forms using a thermo-compressing system. The different composites prepared and their code names are listed in Table 1.

Characterization. The deposition rate of the plasma polymerization process was obtained by measuring the thickness of the layer using a mechanical profilometer (DEKTAK 150) measuring the step between coated and uncoated parts on a silicon substrate. The FTIR spectra were recorded on a Bruker IFS 66v/S spectrometer in transmittance mode with a 4 cm⁻¹ resolution. The background and sample spectra were obtained in the 400−4000 cm⁻¹ wavenumber range using the standard KBr technique.

Table 1. Listing of the Different Samples of This Work

sample	plasma power (W)	HA (wt %)
PLA	0	0
PLA HA 10%	0	10
PLA HA 20%	0	20
PLA HA PPF 20 W 10%	20	10
PLA HA PPF 20 W 20%	20	20
PLA HA PPF 100 W 10%	100	10

Static Time-of-Flight Secondary-Ion Mass Spectrometry. ToF-SIMS data were acquired in positive and negative modes using a ToF-SIMS IV instrument from ION-TOF GmbH. An Ar⁺ 10 keV ion beam was used as an analysis beam at a current of 0.7 pA in the positive mode and 2 pA in the negative mode and rastered over a scan area of $300 \times 300 \ \mu m^2$. Six different locations on the surface were accounted for in the ToF-SIMS analysis. The ToF-SIMS spectra were analyzed with the help of the PCA method using SIMCA-P13 software supplied by Umetrics, Sweden.[29] The peak intensity of the secondary ions was normalized to the total ion count before performing the PCA to correct for the differences in the total secondary ion yield from spectrum to spectrum. The normalized spectra were exported from the acquisition software (SurfaceLab v6.4) to SIMCA-P13 analysis software, which mean-centers and scales the variables. The scaling of all of the peaks inside the ToF-SIMS spectra gives them the same statistical weight, independently of their relative intensity in the spectra. This procedure ensures that the variance in the data is related to chemical differences between samples and not to artifacts in peak intensity.[30]

X-ray Photoelectron Spectroscopy. XPS was also used to characterize the atomic composition of the modified particle surface using an ESCA-5000 (Physical Electronics) Versa Probe system. The following X-ray settings were used: beam size diameter: 200 μm; beam power: 50 W; and voltage: 15 kV. The pressure in the analysis chamber was typically 2.10−6 Pa. The XPS data were collected using monochromatic Al Kα radiation at 1486.6 eV. Photoelectrons were collected at a take-off angle of 45° (normal detection) to the surface normal. Survey (general) spectra were recorded with a 187.85 eV pass energy, a 0.5 eV step, and 40 ms/step.

Water Contact Angle. WCA measurements were realized on a silicon wafer using a drop shape analysis System DSA Mk2 in a static mode at 25 °C by a sessile drop method. For each sample, at least five measurements on different surface locations were averaged.

The modified particles were analyzed by thermogravimetric analysis using a TGA Q500 from TA Instruments under a nitrogen atmosphere. The analysis was done at 10 °C/min from room temperature to 1000 °C.

The thermal properties of the composites were analyzed by differential scanning calorimetry (DSC) using a DSC Q2000 from TA instruments. The analysis was done at 10 °C/min, and a heat/cool/heat program was applied to the sample from −20 to 200 °C. The observation of the thermal transitions of the materials was done on the last cycle.

The thermomechanical analysis of the samples was realized by a DMTA Q800 (TA Instruments) using a multistrain mode at a frequency of 1 Hz and an amplitude of 20 μm in dual cantilever mode. A ramp of 2 °C/min was applied to the sample from −20 to 80 °C. Spectral data analysis was done using the TA Universal analysis.

Dynamic rheological measurements were carried out using an AR-G2 rheometer (TA Instruments) in a parallel-plate (25 mm) configuration at 180 °C under a N_2 atmosphere. Prior to testing, samples were vacuum-dried at 60 °C overnight. Small-amplitude oscillatory experiments (SAOS) were performed in the angular frequency range $0.628 < \omega < 628$ rad/s at 3 % strain (linear viscoelastic regime [LVR]). To ensure sufficient data in the terminal regime, creep-recovery experiments were performed using fresh samples. The compliance data, $J(t)$, were converted into dynamic measurements using the NLREG method.[31]

Morphological evaluations were performed via scanning electron microscopy (SEM) of samples on (modified) HA particles and cryofractured composite cross sections, carbon sputter coated at an accelerating voltage of 10 keV using a JEOL, JSM 6300 (JEOL Ltd., Tokyo, Japan). Statistical analyses were performed using ImageJ software.

Evaluation of Cytotoxicity. Dental pulp-derived stromal cells (DPSCs) of five independent donors were isolated and amplified at a density of 3×10^3 cell/cm² in α-MEM supplemented with 10% decomplemented FBS, 1% penicillin/streptomycin/amphotericin B, and 1% glutamax (v/v, Gibco) and maintained in a humidified atmosphere of 5% CO_2 at 37 °C with a medium change every 2 days. DPSCs were seeded in 24-well plates at 10^4 cells/cm² and cultured for 24 h.

HA PPF 20 W, HA PPF 100 W, and HA powders were incubated for 24 h at 37 °C in supplemented α-MEM at a concentration of 1 mg/mL. Conditioned media were then collected, filtered, and added to seeded DPSCs for 24 h, according to the ISO standard (ISO/EN 10993 part 5 guidelines). The viability of DPSCs was assessed by the WST-1 cell proliferation assay (Roche Diagnostics) in accordance with the manufacturer's protocol. Absorbance was measured at 440 nm using a FLUOstar Omega microplate reader (BMG Labtech) against a background control as the blank. A wavelength of 750 nm was used as the correction wavelength. The lactate dehydrogenase (LDH) released in supernatants was measured according to the manufacturer's protocol (Cytotoxicity detection kit, Roche). The absorbance was read at 492 nm. Finally, the morphology of DPSCs was evaluated following cytoskeleton labeling. Briefly, DPSCs were fixed with 4% (w/v) paraformaldehyde (Sigma-Aldrich) at 37 °C for 10 min and permeabilized with 0.5% (v/v) Triton X-100 for 5 min. Alexa Fluor-488-conjugated phalloidin (1/100 dilution in 0.1% Triton X-100) was used to stain F-actin for 45 min at room temperature. Nuclei were counterstained with 4,6-diamidino-2-phenylindole (DAPI, 100 ng/mL, 1/3 000 dilution) for 5 min. Stained stem cells were mounted and imaged by microscopy (Axiovert 200 M microscope, Zeiss, Oberkochen, Germany, Objective × 20). Image analysis was performed using ImageJ.
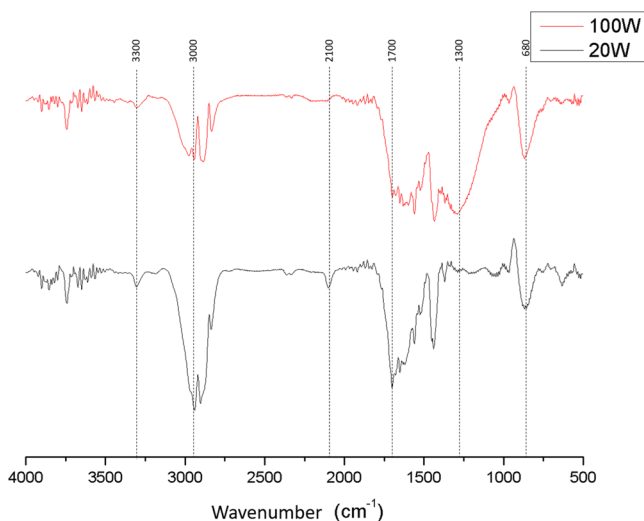
■ RESULTS AND DISCUSSION

To develop the one-shot process for plasma-assisted surface modification of HA particles, acetylene plasma chemistry was first studied on a plane substrate to facilitate the chemical characterization and optimization.

In a first attempt, the deposition rate of the plasma polymerization process was evaluated. The performed DEKTAK studies showed values of 16 nm/min for P = 20 W and 98 nm/min for P = 100 W, suggesting an increase in the decomposition rate at a higher load of energy. In line with the literature, this behavior is explained by a higher production rate of film-forming species in the plasma.[23] Then, the chemical composition of the PPFs was determined. Figure 1 shows the FTIR spectra of the two different PPFs.

For P = 20 W, one can observe the presence of alkyne functions at 3300 and 2100 cm⁻¹, while these functions were shown only at 3300 cm⁻¹ for P = 100 W. These two peaks are related to monosubstituted C−H stretching of the alkyne group. The bending of this C−H function is also present as a sharp function at 680 cm⁻¹. The main difference is the presence of a weak wave at around 2200 cm⁻¹ that can be related to a stretching of the triple bond of the disubstituted alkyne function for the high-power coating. This can be related to a higher fragmentation of the precursor in the plasma on increasing the power, resulting in a more pronounced loss of the chemical integrity of the precursor.

On the other hand, for both PPF, a hydrocarbonated backbone formed by CH₃, CH₂, and CH functions was

**Figure 1.** FTIR spectrum of 500 nm thick PPF deposited for P = 20 W (down, blue) and 100 W (up, red).

Figure 2. TOF-SIMS-positive spectra obtained from 20and 100 W coatings (*, # specific m/z).

Figure 3. Score graph obtained from the PCA analysis of positive spectra (20 and 100 W coatings).

observed at around 3000 cm^{-1} (stretching) and 1500 cm^{-1} (bending), and a broad carbonyl band was observed at 1700 cm^{-1}. The origin of the oxidized functions can be explained by the presence of radicals trapped in the plasma polymer network after their synthesis. As a consequence, after removing the sample from the reactor, these radicals react with oxygen in the ambient air, resulting in the incorporation of oxygen-based functionalities.[32] The broadening of the peak corresponds to the different structures of carbonyl groups (aldehyde, ketone, ester, etc.). The stretching of aromatic bonds also occurs in this area and can also explain the broadness of this band. However, only for P = 100 W, the aromatic C−H in-plane stretch can be observed at around 1200 cm^{-1} in the appearance of a broad wave.

Summarizing the above, these results suggest that (i) both PPFs are mainly formed by alkyl compounds and both present oxidized functions, (ii) the low working power promotes the presence of less fragmented precursors in the film, and/or (iii) the high working power results in the presence of aromatic compounds in the films.

To complete the chemical characterization of the PPF and confirm the previous hypotheses, ToF-SIMS analyses were performed (Figure 2).

As can be seen in Figure 2 and as frequently encountered for PPF, the ToF-SIMS spectra contain numerous signals. Therefore, the difference between the spectrum recorded at 20 and 100 W is hardly visible in this figure, except for several peaks, which display significant differences in relative intensities (see *: C$_2$H$_3^+$ at m/z = 27 and #: C$_7$H$_7^+$ at m/z = 91). To better discriminate the composition of these two samples, principal component analysis (PCA) was performed. This statistical approach has been proven to be an efficient method to assess the main differences in a large amount of data.[29] The score graph obtained from the PCA analysis of positive spectra (20 and 100 W coatings) is represented in Figure 3.

We can clearly observe that the samples prepared at 20 and 100 W display significantly different PC1 scores, revealing their chemical dissimilarity. It is noteworthy that the PCA analysis was performed in parallel for the negative spectra, and for conciseness, the corresponding score graph is not displayed here. Further analysis of the fragments helps to understand the
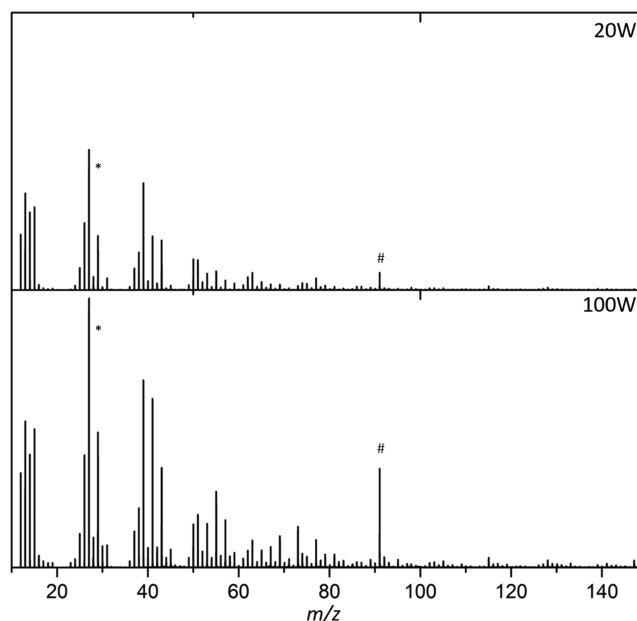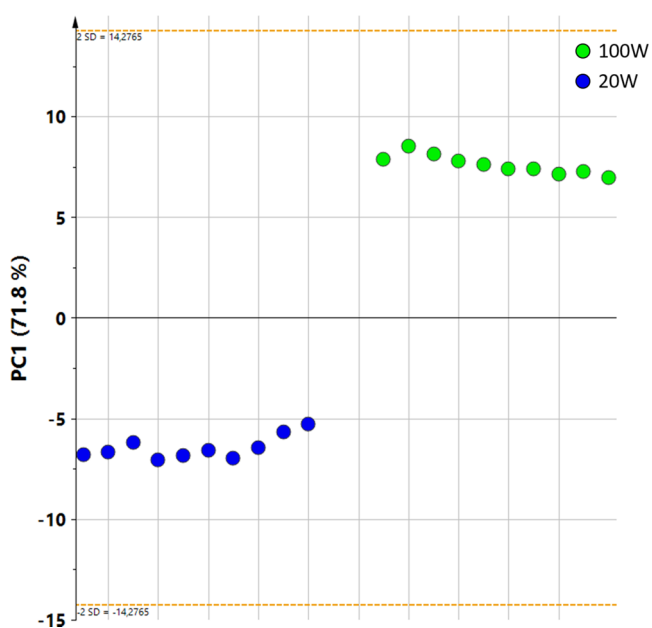
difference in terms of the chemical composition of the coatings. The most relevant ions (positive and negative) are presented in Table S1. Both coatings present alkyl and alkyne moieties as shown in positive and negative ions. Beyond the alkyl moieties, the 100 W sample shows additional aromatic fragments,[33] confirming FTIR spectra observations. Furthermore, a high number of oxygenated ions are found for the 100 W samples resulting from postoxidation reactions in the air. This behavior is attributed to a higher concentration of trapped radicals in the PPF after their synthesis on increasing the power, as is usually observed.[34]

To evaluate the influence of the chemical composition of the PPF on the hydrophilicity of the surface, water contact angle (WCA) measurements were performed. The WCAs of coatings

for P = 20 and 100 W are around 62 ± 3 and 50 ± 3°, respectively. The increase in the hydrophilicity with power is explained considering the chemical composition of the film as, for example, the presence of aromatic species for 100 W PFF. Moreover, the higher concentration of oxygen-based functions for this PPF also contributes to the decrease in the contact angle.

It can be concluded that the power dissipated in the plasma during the process greatly influences the chemical composition of the PFF going from an alkyne/alkyl-rich film to an alkyl/aromatic film with an enriched oxygen surface. The developed and studied methodology was further transferred to HA particles that will play a role in the filler/matrix interface stabilization.

Considering the deposition rate measurements of the plasma polymerization process for both powers on flat substrates and taking into account the specific surface area of the HA microparticles (i.e., 100 m²/g as provided by the supplier), the plasma polymer deposition time was adjusted to obtain a theoretical thickness of 6 nm, assuming a homogeneous covering. Nanometric coating thickness was chosen as the interface between the filler and the matrix is in this range.[13,14] Moreover, the choice of this value was also made considering the long time required for the experiment (more than 20 h of treatment at P = 20 W). The morphological effect of the deposition process can be observed in Figure 4. A change of the surface of the powder could be directly seen by a clear change of color from white to light brown (Figure S2).

As can be seen, the plasma conditions do not induce any modification of the overall morphology of the particles. The
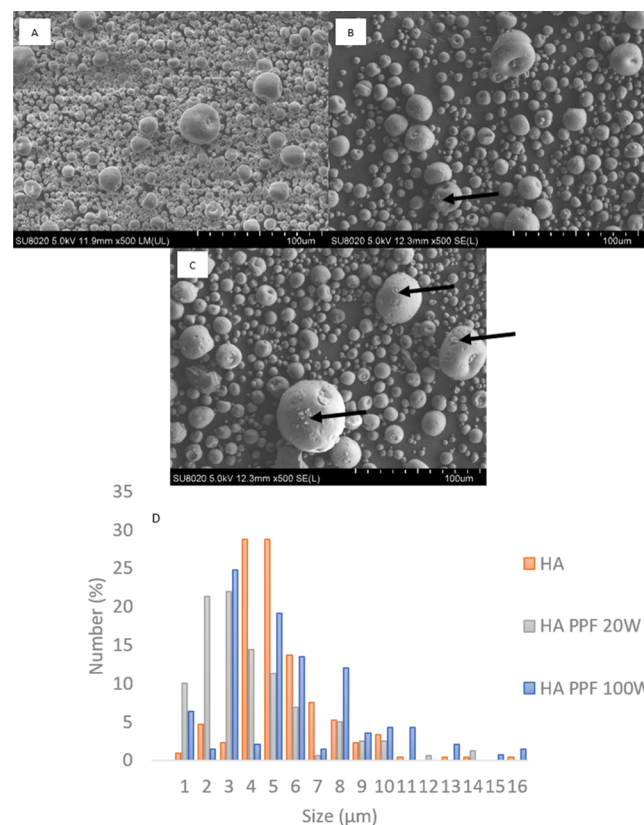
distribution in the size of the particles seems not to be affected by the process (Figure 4D). No erosion of the surface is visible at 20 W, and the particles remain spherical. Small defects on the surface of the big functionalized particles can be seen principally at 100 W, resulting from the higher ionic bombardment. The change of color is an indication of the modification of the surface of the particles going from white to brown, with more dark colors for higher plasma power coating (Figure S2). This organic layer around these particles was analyzed by XPS and thermogravimetric analysis (Figure 5).
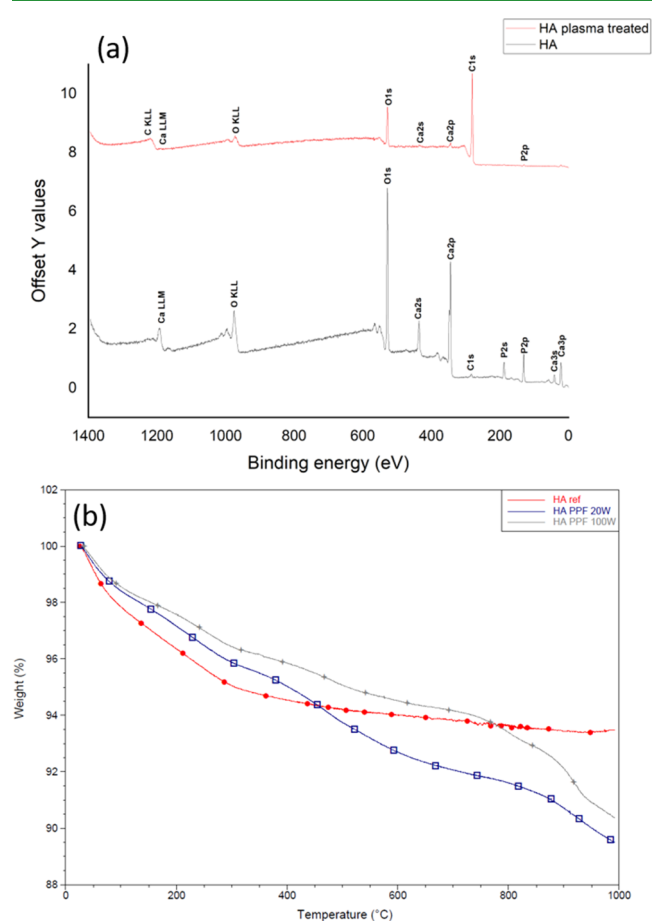
Figure 5. (a) Typical XPS survey of HA ref and plasma-treated particles and (b) TGA analyses of the modified particles.

The XPS analysis of the plasma-treated particles reveals a significant increase in the atomic carbon content (i.e., from 3.6 to 83.4%) accompanied by a decrease in the peaks relative to the HA (i.e., calcium and phosphorus). This is explained by the deposition of the PPF at the surface of the particles.

Regarding the thermogravimetric analysis, the multistep degradation of the modified particles is due to the specificity of the PPF involving several "domains" including alkyl/alkyne chains and aromatic structures. After the thermogravimetric analysis, the powder became white as the unmodified particles, confirming the complete degradation of the organic layer on the surface. Based on the difference of the weight before and after the analysis, the quantity of the organic coating on the particles can be calculated. The quantity seems quite small, which can be easily understood considering the low thickness deposited. In the pristine HA particles, a loss of around 6 wt % is observed and can be related to the high hygroscopic

Figure 4. SEM micrographs of (A) neat μ-HA, (B) HA PPF 20 W, and (C) HA PPF 100 W. (D) Size distribution of the HA reference, HA PPF 20 W HA, and HA PPF 100 W.
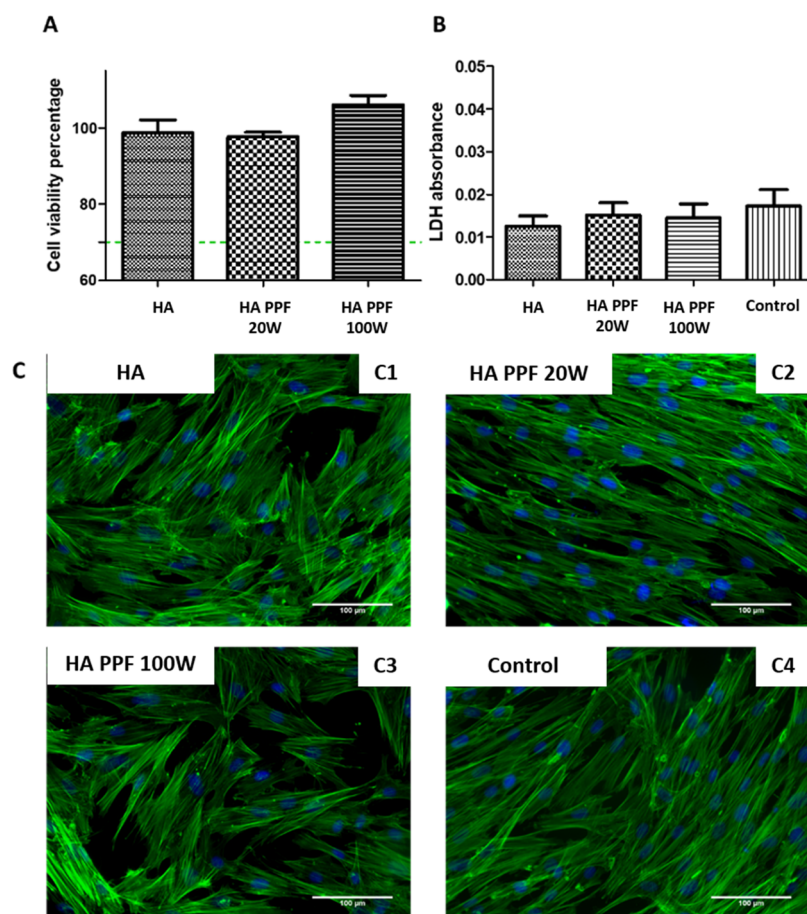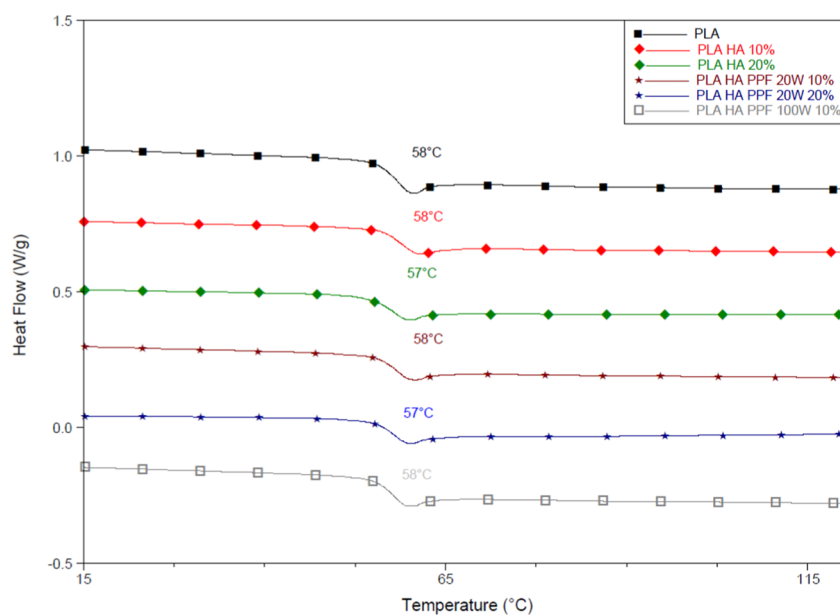
Figure 6. Cytotoxicity tests. (a) Cell viability, (b) LDH absorbance, and (c) morphological analysis of the cells (green: cytoplasm, blue: nucleus).


Figure 7. DSC thermograms of composites.

properties of the HA particles. The organic contents of the 20 and 100 W coated particles were, respectively, 10.5 and 9.6 wt %. These values were further used to calculate the final concentration of ceramic particles in the composites. However, prior to any blending with PLA, the modified HA particles were analyzed to evaluate their potential biological use in

elaboration of material for bone tissue engineering. Biological requirements such as, for example, cytotoxicity tests are necessary to evaluate whether the coating process is harmful.

Cytotoxicity of 20 and 100 W particles was first monitored by the WST-1 proliferation assay and lactate dehydrogenase (LDH) release. The absorption values of the reduced WST-1
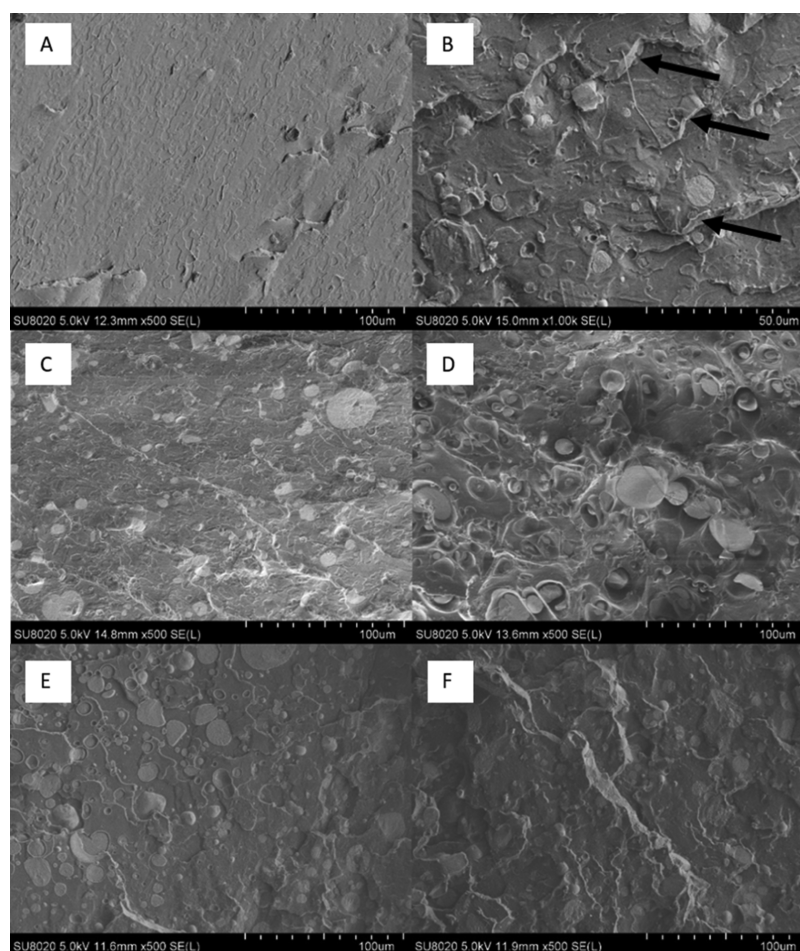
Figure 8. SEM fracture surface of (A) PLA, (B) PLA/HA 10 wt %, (C) PLA/HA PFF 20 W 10 wt %, (D) PLA/HA PPF 100 W 10 wt %, (E) PLA/HA 20 wt %, and (F) PLA/HA PPF 20 W 20 wt %.

reagent normalized to the glass positive control are shown in Figure 6A. Independent on the studied conditions, the mitochondrial activity of DPSCs remained above 70% of the cell viability threshold, considered as an indicator of a cytotoxic phenomenon, according to the ISO standard (ISO/EN 10993 part 5 guidelines). Furthermore, no significant differences in LDH accumulation in the supernatant were noticed (Figure 6B). Finally, F-actin cytoskeleton labeling showed that DPSCs in the presence of HA particles presented a fibroblastic shape similar to that of the control (Figure 6C). Taken together, these results highlighted the absence of DPSC damage in the presence of HA particles.

The coating is successfully present around the particles as proven by XPS and TGA and it does not destroy their morphology or induce any harmful effect on cells. These particles are then suitable as fillers of bone tissue engineering in PLA.

The three different particles (HA reference, HA PPF 20 W, and HA PPF 100 W) were blended with PLA by the extrusion process. Amorphous PLA was used to clearly establish the role of the PPF coating in the mechanical properties of the HA/PLA composite without exerting any positive or negative HA influence on PLA crystallinity. These composites were first analyzed by DSC (Figure 7). The different thermograms of the composites did not show significant differences between the samples. The polymer remains glassy and has no plasticizing effect (no shift of T_g toward lower temperatures) compared to

the use of a low-molecular-weight surfactant.[35] As no further influence of HA modification on PLA thermal properties and/ or crystallinity was expected, X-ray scattering was not performed.

SEM analysis was performed to investigate the morphology, the mode of fracture, and the homogeneity of the dispersion of the particles inside the PLA matrix. As can be seen (Figure 8A), a typical "hackled" pattern surface topography, ascribed to the well-reported brittle behavior of PLA resin, was observed for PLA samples.[36] The addition of HA particles (10 wt %) changes drastically the morphology of the PLA fractured surface. That is, in Figure 8B, the fractured surface is rougher, and plastic tearing is highlighted by black arrows. The particles do not appear to be well dispersed and present some agglomeration. This effect is even more pronounced when the quantity of HA is increased up to 20 wt % (Figure 8E). A weak interfacial strength between the hydrophilic filler and the hydrophobic matrix may explain the agglomerate formation and the weak bonding as discussed by Neuendorf et al.[37] As described above, the plasma process can be used to modify the WCA angle of a surface. Similar behavior can be expected on the particles and can be used to explain the behavior of the composites. At 20 W, the WCA of the coating reaches 62°, which is closer to that of PLA. The interface strength is then increased, and we can observe well-dispersed particles with no tendency of agglomeration. Moreover, an almost flat surface is obtained, inducing good transfer of the stress from the matrix
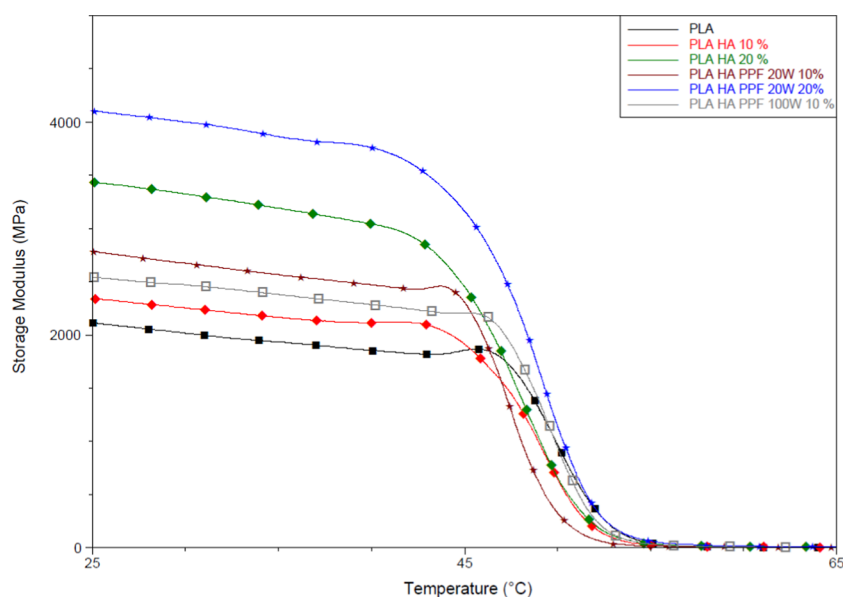
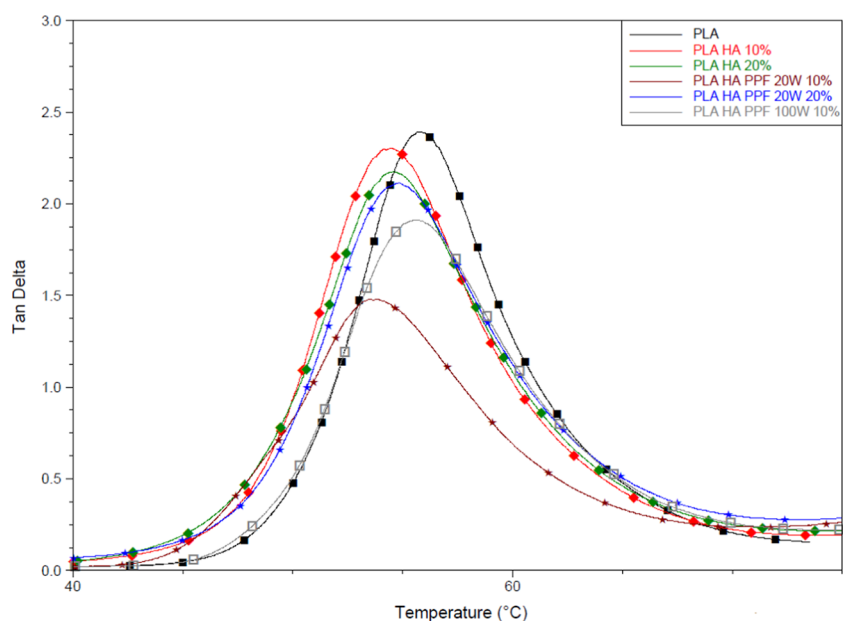**Figure 9.** DMA thermograms of the composites (storage modulus).

Figure 10. DMA thermograms of the composites (tan δ).

to the reinforcing phase. Even at 20 wt % of ceramic particles, no tendency of agglomeration was observed (Figure 8F). However, the particles modified at 100 W present a WCA of 50 °C, which is closer to that of native HA. The particles appear completely unbounded from the matrix (Figure 8D). The PLA matrix appears highly deformed around the crack, and interfacial slip is clearly observed. The functionalization performed at 100 W weakens the interfacial bonding between the PLA and the filler matrix. However, the difference in WCA cannot explain why the interfacial bonding seems to be higher in the neat mixing than the modified particle. The WCA can be used to qualify the interfacial bonding through chemical interaction only. However, another factor leading to the interaction bonding is the physical interactions.[38] This one is based on mechanical interlocking and steric effects. The physical bonding can explain the difference between the binary PLA/HA mix and the one with the particles modified at 100

W. The unmodified particles possess OH functions on the surface, 2.6 groups/nm^2. These groups can, to some extent, interact with the PLA chain by physical interaction and delay the interfacial slipping of the matrix. However, when we modified the particles, a very hard and stiff coating covered the particles, excluding the possibility of physical bonding of the modified surface. The result is a complete slip of the matrix even if the WCA of this coating is higher than those of pure HA particles.

To better monitor the HA/PLA interactions at the interface, the viscoelastic behavior and the rheological behavior of the composites were monitored. Dynamical mechanical thermal analysis, e.g., the evolution of the storage modulus (E') and the mechanical loss factor (tan δ), was first performed. The effects of the surface functionalization on the storage modulus (Figure 9) and mechanical loss factor (Figure 10) were observed.

3074

The presence of ceramic particles has a beneficial effect on the mechanical modulus as depicted in Figure 9. The comparison of the moduli of the materials is shown in Table 2 at 37 °C. Since all of the samples are amorphous, the higher

Table 2. Storage Moduli at 37 °C (E), Temperature of the Damping Peak ($T_{\tan \delta}$), and Damping Factor ($\tan \delta$) of Neat PLA and its Composites with Unmodified and Modified HAs

code	$E'_{37 °C}$ (MPa)	$T_{\tan \delta}$ (°C)	$\tan \delta$
PLA	1900	56.0	2.389
PLA HA 10 wt %	2100	54.5	2.302
PLA HA 20 wt %	3100	54.5	2.172
PLA HA PPF 20 W 10 wt %	2500	54.0	1.477
PLA HA PPF 20 W 20 wt %	3800	54.5	2.109
PLA HA PPF 100 W 10 wt %	2300	55.5	1.912

moduli exhibited by the PLA/plasma-modified HA composites can be attributed to an improved interface, leading to an increase in the quality of the stress transfer from the matrix to the ceramic particles. Especially for the materials filled with 20 wt % of modified particles (at 20 W), the storage modulus (3.8 GPa) has doubled from the unfilled polymer (1.9 GPa). Moreover, the storage modulus for the unmodified particles is significantly lower (3.1 GPa), proving the beneficial effect of the coating on the final mechanical properties of the materials.[14,27] It should be noted that it has been proven that the mechanical properties have a huge impact on the quality of the final regenerated bone.[6]

The addition of particles does not affect the transition α (related to the glass temperature as in ref 39) significantly, as determined by $\tan \delta$, which correlates with the results from DSC. The damping factor can be also used to characterize the filler/matrix interface. Ko et al.[40] showed that a decrease in the damping peak can be attributed to higher interface adhesion. Indeed, the $\tan \delta$ can be related to the interfacial adhesion

because this data is a true indication of molecular motion. The molecular motion will be influenced by the interfacial adhesion.[38] Besides, the energy dissipation in a composite occurs on the interface, so a strong interface means low dissipation with a restricted movement of the chains around the filler and effective stress transfer. In our work, adding HA particles decreases the molecular motion and so the damping peak decreases. The decrease is more pronounced for the modified particle because of the stress transfer in these better filler/matrix interface systems. The influence of the working plasma power can be also observed with a lower $\tan \delta$ for the particles modified at 20 W, proving once again the better interface. Moreover, increasing the filler in the composites leads to an increase in the damping peak. The same observation is made on the TGA thermograms, where only the modified particles at 20 W show an increase of the thermal properties of the materials (Figure S5). The modified particles remain slightly lower in $T_{\tan \delta}$ than the unmodified particles. The shift of the $T_{\tan \delta}$ remains small but a decrease can be explained by the introduction of the filler as an increase of the surface of the polymer due to the introduction of the charge.[41]

Rheological properties were investigated to gain an insight into the interfacial interactions between the inorganic HA solid particle and the PLA host matrix. Figure 11 shows the ω dependence of the complex viscosity, $|\eta^*|$, and the storage modulus, G', of all of the considered composites. After adding modified HA particles, changes in the interfacial interactions between both components can be studied using the weighted relaxation spectrum, as shown in Figure 11c. It was calculated using both dynamic moduli (i.e., the storage, G', and loss, G'', modulus) from the linear relaxation spectrum, H(λ).[31] The position of the relaxation peak(s) is reported to be indicative of the strength of the interfacial adhesion as it reflects the time distribution of chain relaxation. That is, the stronger the interfacial adhesion, the longer time the relaxation of the PLA macromolecules surrounding the HA particles takes up.
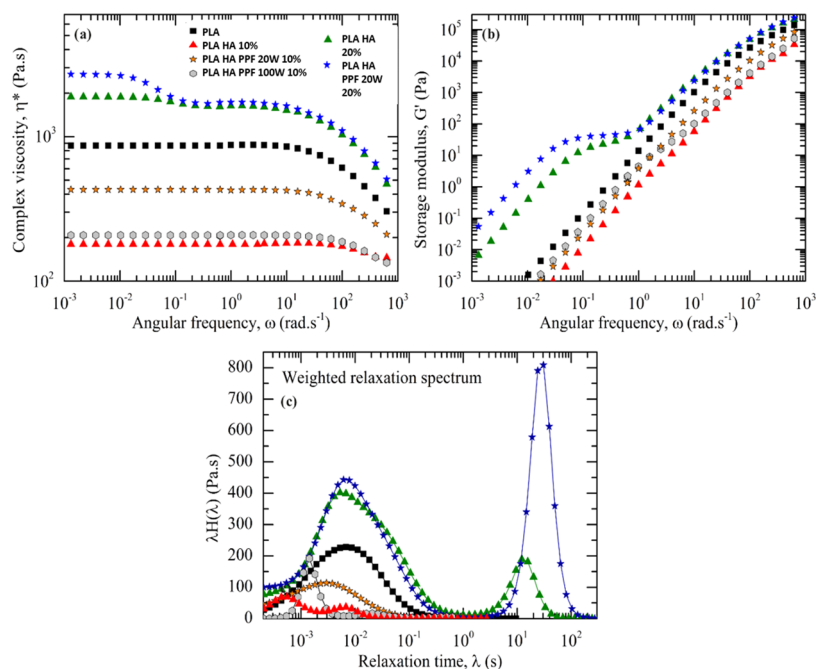
Figure 11. ω Dependence of the (a) complex viscosity and (b) storage modulus together with the (c) weighted relaxation spectra at 180 °C.

PLA exhibited the expected typical pseudoplastic fluid behavior with a monomodal distribution of relaxation time, λ, centered at around 7.10^{-3} s. Adding 10 wt % HA particles led to a significant drop in the complex viscosity values, and the onset of the shear-thinning behavior shifted to higher ω. Moreover, the monomodal distribution of relaxation times displayed by PLA changed to a bimodel one for PLA HA 10% composites. The main relaxation peak shifted to shorter relaxation times (from 7.10^{-3} to 5.10^{-4} s), and the overall distribution was narrowed, suggesting an apparent speeding up of relaxation of the host matrix. These results can be ascribed to the well-reported incompatibility and poor interfacial interaction between the micrometer-sized solid particles and the PLA macromolecules, which induced interfacial slip and lowered the PLA viscous resistance.[39]

In contrast, adding 20 wt % HA particles increased $|\eta^*|$ values over the whole experimental window and broadened the relaxation spectrum of PLA, wherein an additional relaxation peak at longer relaxation times (≈ 11.8 s) appears. Since HA particles exhibited similar surface properties between PLA HA 10% and PLA HA 20% samples, this behavior indicated that physical constraints induced a second relaxation mechanism. That is, while the unperturbed PLA chains are free to relax by relatively fast self-diffusion processes, the lowered thickness of the interlayer between particles restricted the molecular mobility of the PLA chains surrounding particles that must relax through other longer mechanisms. In the low ω region, the retarded macromolecular relaxation enhanced the solidlike behavior of the melt, as confirmed by the higher G' values than PLA.

The results of rheological property measurements indicated that the surface modification on HA with plasma 20 W led to an improvement of the complex viscosity as well as storage modulus values of the corresponding unmodified PLA/HA composites. Since the hydrophobicity of HA particles was enhanced with plasma 20 W, the corresponding enhancement can be ascribed to improved interfacial interactions between the molten polymer and the particle surface, which minimized interfacial slip, as already reported elsewhere.[42] In the weighted relaxation spectra, these trends were reflected in the time distribution of chain relaxations. While the main relaxation peak of the PLA HA PPF 20 W 10% sample shifted to longer relaxation times than PLA HA 10% (from 5.10^{-4} to 3.10^{-3}), the second relaxation time exhibited by PLA HA PPF 20 W 20% samples increased from 11.8 s to 31.7 s as compared to PLA HA 20% ones. According to the above-discussed results, surface modification of HA particles using plasma 100 W did not improve the interfacial adhesion between both components. These results are consistent with the proposed possibility to tune filler matrix interface properties by a plasma polymer coating.

CONCLUSIONS

The present study successfully developed HA/PLA composites of improved filler−matrix interfacial bonding and enhanced mechanical performances with at least preserved biocompatibility of bone implants possibly based on HA/PLA. For this, one-shot surface functionalization of HA via plasma polymerization is developed for fine tuning the hydrophobicity of HA particles prior to their introduction into a PLA matrix via extrusion. Plasma power was found to be a sufficient parameter for modulating the surface chemistry and the related hydrophilicity/hydrophobicity of the HA surface. It is

noteworthy that the amount of PPF and the morphology of the (modified) HA were found to insignificantly vary with plasma power. Cytotoxicity tests revealed preserved biocompatibility. Contact angle measurements and morphological and rheological analyses showed that a working power of 20 W promoted more hydrophobic surfaces and a better HA/PLA interface. Dynamic mechanical analyses revealed improved mechanical properties for the modified HA/PLA composites in comparison to the neat HA/PLA. This work opens a route toward further one-shot development of improved scaffolds for bone tissue engineering.

ASSOCIATED CONTENT

Supporting Information

The Supporting Information is available free of charge at https://pubs.acs.org/doi/10.1021/acsabm.0c01429.

Experimental setup of the plasma functionalization process; most important ions present during the analysis of the coating; visual aspects of (a) the HA reference, (b) HA PPF 20 W, and (c) HA PPF 100 W; GPC curves of the different composites; size distribution of the neat particles and the composites of 20 wt % of filler; and TGA thermograms of the neat PLA and the composites (PDF)

AUTHOR INFORMATION

Corresponding Authors

Rosica Mincheva − *Laboratory of Polymeric and Composite Materials (LPCM), CIRMAP, University of Mons, B-7000 Mons, Belgium*; Email: rosica.mincheva@umons.ac.be

Jean-Marie Raquez − *Laboratory of Polymeric and Composite Materials (LPCM), CIRMAP, University of Mons, B-7000 Mons, Belgium*; orcid.org/0000-0003-1940-7129; Email: jean-marie.raquez@umons.ac.be

Authors

Xavier Carette − *Laboratory of Polymeric and Composite Materials (LPCM), CIRMAP, University of Mons, B-7000 Mons, Belgium*; orcid.org/0000-0002-1317-3264

Laeticia Dhond − *Laboratory of Polymeric and Composite Materials (LPCM), CIRMAP, University of Mons, B-7000 Mons, Belgium; Chimie des Interactions Plasma Surface (ChIPS), CIRMAP, University of Mons, B-7000 Mons, Belgium*

Axel Hemberg − *Materia-Nova Research Center, Parc Initialis, B-7000 Mons, Belgium*

Damien Thiry − *Chimie des Interactions Plasma Surface (ChIPS), CIRMAP, University of Mons, B-7000 Mons, Belgium*; orcid.org/0000-0001-6703-1512

Jonathan Cailloux − *Centre Català del Plàstic (CCP), Universitat Politécnica de Catalunya-Barcelona Tech (EEBE-UPC), 08019 Barcelona, Spain*; orcid.org/0000-0003-3785-0829

Orlando Santana Perez − *Centre Català del Plàstic (CCP), Universitat Politécnica de Catalunya-Barcelona Tech (EEBE-UPC), 08019 Barcelona, Spain*

Damien Cossement − *Materia-Nova Research Center, Parc Initialis, B-7000 Mons, Belgium*

Marie Dubus − *EA 4691 Biomatériaux et Inflammation en Site Osseux (BIOS), Université de Reims Champagne-Ardenne, 51100 Reims, France; UFR d'odontologie,*

Universite' de Reims Champagne Ardenne, 51100 Reims, France

Halima Kerdjoudj − EA 4691 Biomatériaux et Inflammation en Site Osseux (BIOS), Université de Reims Champagne-Ardenne, 51100 Reims, France; UFR d'odontologie, Universite' de Reims Champagne Ardenne, 51100 Reims, France; orcid.org/0000-0002-8072-9728

Rony Snyders − Chimie des Interactions Plasma Surface (ChIPS), CIRMAP, University of Mons, B-7000 Mons, Belgium; Materia-Nova Research Center, Parc Initialis, B-7000 Mons, Belgium

Complete contact information is available at:
https://pubs.acs.org/10.1021/acsabm.0c01429

Notes
The authors declare no competing financial interest.

REFERENCES

(1) Akindoyo, J. O.; Beg, M. D. H.; Ghazali, S.; Heim, H. P.; Feldmann, M. Effects of Surface Modification on Dispersion, Mechanical, Thermal and Dynamic Mechanical Properties of Injection Molded PLA-Hydroxyapatite Composites. *Composites, Part A* 2017, 103, 96−105.
(2) Jahan, K.; Tabrizian, M. Composite Biopolymers for Bone Regeneration Enhancement in Bony Defects. *Biomater. Sci.* 2016, 4, 25−39.
(3) Li, S. Hydrolytic Degradation Characteristics of Aliphatic Polyesters Derived from Lactic and Glycolic Acids. *J. Biomed. Mater. Res.* 1998, 48, 342−353.
(4) Elsawy, M. A.; Kim, K.-H.; Park, J.-W.; Deep, A. Hydrolytic Degradation of Polylactic Acid (PLA) and Its Composites. *Renewable Sustainable Energy Rev.* 2017, 79, 1346−1352.
(5) Lin, A. S. P.; Barrows, T. H.; Cartmell, S. H.; Guldberg, R. E. Microarchitectural and Mechanical Characterization of Oriented Porous Polymer Scaffolds. *Biomaterials* 2003, 24, 481−489.
(6) Grøndahl, L.; Jack, K. S.; Goonasekera, C. S. *Composite Materials for Bone Repair*, 2nd ed.; Elsevier Ltd., 2017.
(7) Stamm, M. *Polymer Surfaces and Interfaces: Characterization, Modification and Applications*; Springer-Verlag Berlin Heidelberg, 2008.
(8) Li, J.; Lu, X. L.; Zheng, Y. F. Effect of Surface Modified Hydroxyapatite on the Tensile Property Improvement of HA / PLA Composite. *Appl. Surf. Sci.* 2008, 255, 494−497.
(9) Hong, Z.; Qiu, X.; Sun, J.; Deng, M.; Chen, X.; Jing, X. Grafting Polymerization of L-Lactide on the Surface of Hydroxyapatite Nano-Crystals. *Polymer* 2004, 45, 6699−6706.
(10) Hong, Z.; Zhang, P.; He, C.; Qiu, X.; Liu, A.; Chen, L.; Chen, X.; Jing, X. Nano-Composite of Poly(l-Lactide) and Surface Grafted Hydroxyapatite: Mechanical Properties and Biocompatibility. *Bio-materials* 2005, 26, 6296−6304.

(11) Hasan, M. S.; Ahmed, I.; Parsons, A. J.; Walker, G. S.; Scotchford, C. A. The Influence of Coupling Agents on Mechanical Property Retention and Long-Term Cytocompatibility of Phosphate Glass Fibre Reinforced PLA Composites. *J. Mech. Behav. Biomed. Mater.* 2013, 28, 1−14.
(12) Takayama, T.; Todo, M. Improvement of Fracture Properties of Hydroxyapatite Particle Filled Poly(l-Lactide)/Poly(ε-Caprolac-tone) Biocomposites Using Lysine Tri-Isocyanate. *J. Mater. Sci.* 2010, 45, 6266−6270.
(13) Liu, Z.; Zhao, F.; Jones, F. R. Optimising the Interfacial Response of Glass Fibre Composites with a Functional Nanoscale Plasma Polymer Coating. *Compos. Sci. Technol.* 2008, 68, 3161−3170.
(14) Marks, D. J.; Jones, F. R. Plasma Polymerised Coatings for Engineered Interfaces for Enhanced Composite Performance. *Composites, Part A* 2002, 33, 1293−1302.
(15) Kim, H.-W. Biomedical Nanocomposites of Hydroxyapatite/Polycaprolactone Obtained by Surfactant Mediation. *J. Biomed. Mater. Res., Part A* 2007, 83A, 169−177.
(16) Misra, D. N. Adsorption of Polyacrylic Acids and Their Sodium Salts on Hydroxyapatite: Effect of Relative Molar Mass. *J. Colloid Interface Sci.* 1996, 181, 289−296.
(17) Rees, S. G.; Hughes Wassell, D. T.; Embery, G. Interaction of Glucuronic Acid and Iduronic Acid-Rich Glycosaminoglycans and Their Modified Forms with Hydroxyapatite. *Biomaterials* 2002, 23, 481−489.
(18) Mohapatra, A. K.; Mohanty, S.; Nayak, S. K. Effect of PEG on PLA/PEG Blend and Its Nanocomposites: A Study of Thermo-Mechanical and Morphological Characterization. *Polym. Compos.* 2014, 35, 283−293.
(19) Qiu, X.; Chen, L.; Hu, J.; Sun, J.; Hong, Z.; Liu, A.; Chen, X.; Jing, X. Surface-Modified Hydroxyapatite Linked by L-Lactic Acid Oligomer in the Absence of Catalyst. *J. Polym. Sci., Part A: Polym. Chem.* 2005, 43, 5177−5185.
(20) Hong, Z.; Qiu, X.; Sun, J.; Deng, M.; Chen, X.; Jing, X. Grafting Polymerization of L-Lactide on the Surface of Hydroxyapatite Nano-Crystals. *Polymer* 2004, 45, 6699−6706.
(21) Wang, Y.; Dai, J.; Zhang, Q.; Xiao, Y.; Lang, M. Applied Surface Science Improved Mechanical Properties of Hydroxyapatite / Poly (☐ -Caprolactone) Scaffolds by Surface Modification of Hydrox-yapatite. *Appl. Surf. Sci.* 2010, 256, 6107−6112.
(22) Thiry, D.; Reniers, F.; Snyders, R. A Joint Mechanistic Description of Plasma Polymers Synthesized at Low and Atmospheric Pressure. *Surf. Modif. Polym.* 2019, 67−106.
(23) Thiry, D.; Konstantinidis, S.; Cornil, J.; Snyders, R. Plasma Diagnostics for the Low-Pressure Plasma Polymerization Process: A Critical Review. *Thin Solid Films* 2016, 606, 19−44.
(24) Friedrich, J. Mechanisms of Plasma Polymerization−Reviewed from a Chemical Point of View. *Plasma Processes Polym.* 2011, 8, 783−802.
(25) Akhavan, B.; Jarvis, K.; Majewski, P. Plasma Polymerization of Sulfur-Rich and Water-Stable Coatings on Silica Particles. *Surf. Coat. Technol.* 2015, 264, 72−79.
(26) Asadian, M.; Onyshchenko, I.; Thiry, D.; Cools, P.; Declercq, H.; Snyders, R.; Morent, R.; De Geyter, N. Thiolation of Polycaprolactone (PCL) Nanofibers by Inductively Coupled Plasma (ICP) Polymerization: Physical, Chemical and Biological Properties. *Appl. Surf. Sci.* 2019, 479, 942−952.
(27) Petisco-Ferrero, S.; Pérez Álvarez, L.; Ruiz-Rubio, L.; Vilas Vilela, J. L.; Sarasua, J. R. Plasma Poly(Acrylic Acid) Compatibilized Hydroxyapatite-Polylactide Biocomposites for Their Use as Body-Absorbable Osteosynthesis Devices. *Compos. Sci. Technol.* 2018, 161, 66−73.
(28) Nichols, H. L.; Zhang, N.; Zhang, J.; Shi, D.; Bhaduri, S.; Wen, X. Coating Nanothickness Degradable Films on Nanocrystalline Hydroxyapatite Particles to Improve the Bonding Strength between Nanohydroxyapatite and Degradable Polymer Matrix. *J. Biomed. Mater. Res., Part A* 2007, 82A, 373−382.

(29) Eriksson, L. *Multi- and Megavariate Data Analysis Basic Principles and Applications*, 3rd ed.; MKS Umetrics AB: Malmö, Sweden, 2013.

(30) Cossement, D.; Renaux, F.; Thiry, D.; Ligot, S.; Francq, R.; Snyders, R. Chemical and Microstructural Characterizations of Plasma Polymer Films by Time-of-Flight Secondary Ion Mass Spectrometry and Principal Component Analysis. *Appl. Surf. Sci.* **2015**, *355*, 842−848.

(31) Honerkamp, J.; Weese, J. A nonlinear regularization method for the calculation of relaxation spectra. *Rheologica Acta* **1993**, *32*, 65−73.

(32) Gengenbach, T. R.; Griesser, H. J. Aging of 1, 3-diaminopropane Plasma-deposited Polymer Films: Mechanisms and Reaction Pathways. *J. Polym. Sci., Part A: Polym. Chem.* **1999**, *37*, 2191−2206.

(33) Briggs, D. *Surface Analysis of Polymers by XPS and Static SIMS*; Cambridge University Press, 1998.

(34) Ershov, S.; Khelifa, F.; Dubois, P.; Snyders, R. Derivatization of Free Radicals in an Isopropanol Plasma Polymer Film: The First Step toward Polymer Grafting. *ACS Appl. Mater. Interfaces* **2013**, *5*, 4216−4223.

(35) Chaubey, A.; Aadil, K. R.; Jha, H. Synthesis and Characterization of Lignin-Poly Lactic Acid Film as Active Food Packaging Material. *Mater. Technol.* **2020**, 1−9.

(36) Hong, Z.; Zhang, P.; He, C.; Qiu, X.; Liu, A.; Chen, L.; Chen, X.; Jing, X. Nano-Composite of Poly(L-Lactide) and Surface Grafted Hydroxyapatite: Mechanical Properties and Biocompatibility. *Biomaterials* **2005**, *26*, 6296−6304.

(37) Neuendorf, R. E.; Saiz, E.; Tomsia, A. P.; Ritchie, R. O. Adhesion between Biodegradable Polymers and Hydroxyapatite: Relevance to Synthetic Bone-like Materials and Tissue Engineering Scaffolds. *Acta Biomater.* **2008**, *4*, 1288−1296.

(38) Brocks, T.; Cioffi, M. O. H.; Voorwald, H. J. C. In *Effects of Interfacial Adhesion on Thermal and Mechanical Properties*, Venice, Italy, June 24−28, 2012.

(39) Diao, H.; Si, Y.; Zhu, A.; Ji, L.; Shi, H. Surface Modi Fi Ed Nano-Hydroxyapatite / Poly (Lactide Acid) Composite and Its Osteocyte Compatibility. *Mater. Sci. Eng., C* **2012**, *32*, 1796−1801.

(40) Ko, Y. S.; Forsman, W. C.; Dziemianowicz, T. S. Carbon Fiber-Reinforced Composites: Effect of Fiber Surface on Polymer Properties. *Polym. Eng. Sci.* **1982**, *22*, 805−814.

(41) Wilberforce, S. I. J.; Finlayson, C. E.; Best, S. M.; Cameron, R. E. The Influence of Hydroxyapatite (HA) Microparticles (m) and Nanoparticles (n) on the Thermal and Dynamic Mechanical Properties of Poly-l-Lactide. *Polymer* **2011**, *52*, 2883−2890.

(42) Šupová, M. Problem of Hydroxyapatite Dispersion in Polymer Matrices: A Review. *J. Mater. Sci.: Mater. Med.* **2009**, *20*, 1201−1213.